Solar Array "Hot-Spot" Testing and Analysis

Peter Papula*
RCA Astro-Electronics, Princeton, New Jersey
and
Carole Stowell†
General Electric Company, Philadelphia, Pennsylvania

The environmental testing techniques used in evaluating a space solar array operating under simulated failure modes are discussed. These failure modes cause a local heating phenomenon of solar arrays known as a "hot spot" and are major design obstacles. The empirically derived surface temperature of the solar array is compared to the time-dependent thermal analysis. Special attention is given to the calibration of the infrared scanner used to monitor the solar array surface and the interpretation of its data into meaningful temperatures of a surface with an emittance less than one.

Nomenclature

$AI12_i$ = incident sunlit area, in.^{2}
C_{pi} = specific heat, W/s·lb·°C
K_{ij} = conductive coupling factor, W/°C
Q_i = internal dissipation, W = $f(T_i)$
R_{ij} = radiation coupling factor, in.^{2}
R_{is} = radiation coupling to space, in.^{2}
s_i = solar constant, W/in.^{2}
T_A = temperature of the solar array
T_{dA} = apparent temperature of the solar array as seen by the AGA 780 Thermovision (infrared scanner)
T_B = temperature of the black-body radiator
T_{dB} = apparent temperature of the black body radiator as seen by the AGA 780, the calibration graph equates T_{dB} with T_B
T_i = temperature of node i, K
w_i = weight, lb
W_A = computed radiation from a solar array
W_{dA} = radiation as seen by AGA 780 from viewing the solar array
W_B = computed radiation from a black body of temperature T_B
W_{dB} = radiation from a black-body radiator as seen by the AGA 780
W_{BG} = radiation contribution from the background having an "effective" black-body temperature of T_{BG}
α_i = solar absorptance
ϵ_A = emittance of the solar array
ϵ_i = emittance of the ith body
η_i = solar cell efficiency
θ = Stefan-Boltzmann constant
θ_i = angle between surface normal and sun vector, deg
τ = transmission coefficient of radiation through the salt window

Introduction

A LOCAL heating phenomenon of a solar array, known as the "hot-spot" failure mode, is a major concern in solar array design. Although much has been written about hot-spot analysis techniques[1-3] and cell characteristics,[4] the analysis presented herein, unlike others, is time dependent and has specific parameters pertaining to the solar cell reverse characteristics. The time dependent computational analysis was compared to an experimental test utilizing the specific electrical characteristics of the individual solar cells. Figure 1 is a sketch of a solar array illustrating possible "hot-spot" occurrences.

"Hot spots" can occcur when one or more of several solar cells in parallel in a solar array fails open. The remaining cells in parallel to the failed cell must necessarily pass more current. For example, if one cell of five in parallel opens, each of the remaining four in parallel with the open cell must carry 1.25 times the normal cell current.

Figure 2 is a graph of the current vs voltage characteristics of a typical solar cell. The horizontal dotted line is drawn at the level of 1.25 × (normal cell current). When the current that must be passed is greater than the cell short circuit current (I_{sc}), the voltage shifts into the negative portion of the current-voltage (I-V) characteristic and the solar cells become power dissipators instead of power sources. Tests were devised to simulate the failure modes and conditions that cause cell reversals leading to overheating of the reversed solar cells.

Test Preparation

Solar Cell Characterization

An accurate profile of each solar cell's forward and reverse characteristics is necessary for determining power dissipation before the cell is installed in the test array. A total of 40 carefully identified cells were selected at random for the characterization test.

Test Procedure

1) Calibrate the solar simulator at 28°C and one air mass zero (AMO), the level of solar radiance present beyond the Earth's atmosphere.
2) Record illuminated cell I-V curve.
3) Connect temperature forcing unit, thermocouple, and temperature indicator to the test fixture as shown in the schematic of Fig. 3.
4) Connect the regulated power supply, load box, and X-Y recorder to the test fixture.
5) Adjust the temperature of the test fixture to 25, 50, 75, 100, 150, 175, and 200°C, consecutively.
6) Place the cell for test on the fixture and introduce vacuum.
7) Adjust the power supply to obtain I-V curves of 0-25 V.
8) Cover the solar cell and repeat step 7 to obtain the dark reverse bias curve.

Presented as Paper 85-1080 at the AIAA 20th Thermophysics Conference, Williamsburg, VA, June 19-21, 1985; revision received March 14, 1986.

*Senior Member, Technical Staff.
†Electrical Engineer, Space Systems Division/RSO.

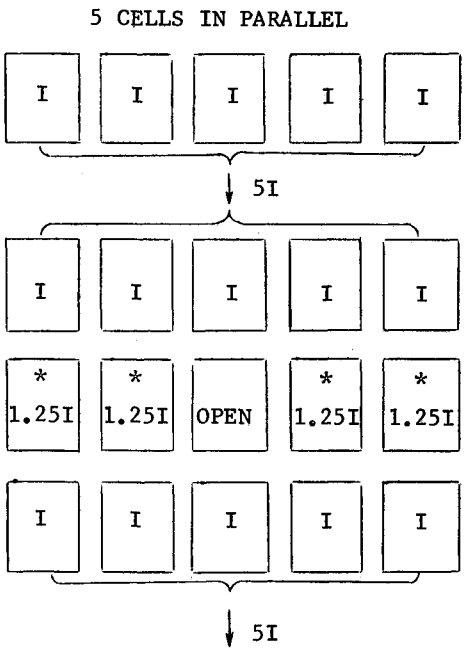

Fig. 1 Hot-spot occurrence (marked by *).

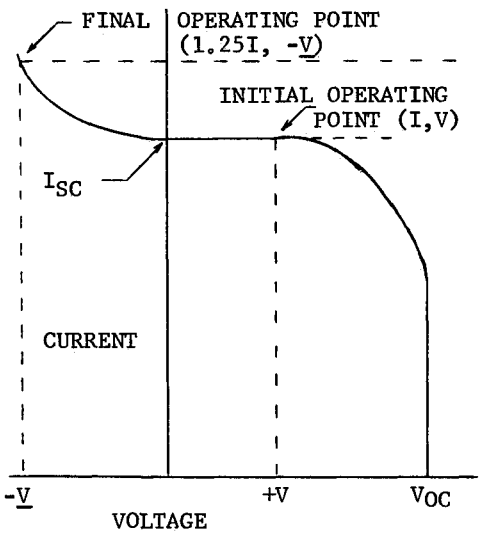

Fig. 2 Change in cell operating point.

Results

The reverse characteristics are independent of the forward characteristics.

The reverse characteristics of the solar cells are parameters that are not controlled during the manufacturing process and should be expected to vary widely within any lot of cells due to the large *P/N* junction.

Current passage of a fixed-voltage, reverse-biased solar cell increases with temperature, tending to stabilize the hot-spot effect. Typical forward illuminated and reverse dark characteristic cell test data are shown in Figs. 4 and 5.

Solar Array Assembly and Pre-Test Characterization

The 5 × 9 array was assembled to accommodate an extreme case of "hot-spot" failure mode. On a nine-cell string containing the "failure cell," all but one of the cells contained average reverse cell characteristics. The remaining cell was selected to have a very leaky, or high reverse current, effecting the anticipated largest power dissipation. The array was subsequently instrumented with thermocouples to monitor bulk temperatures.

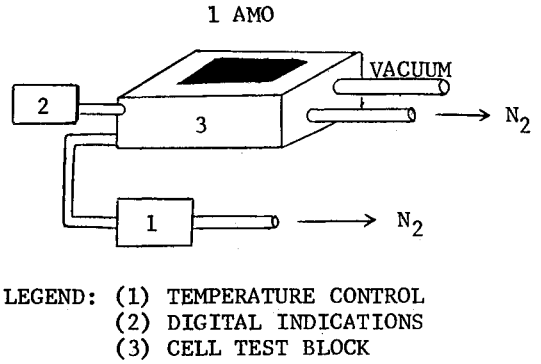

Fig. 3 Solar cell test fixture.

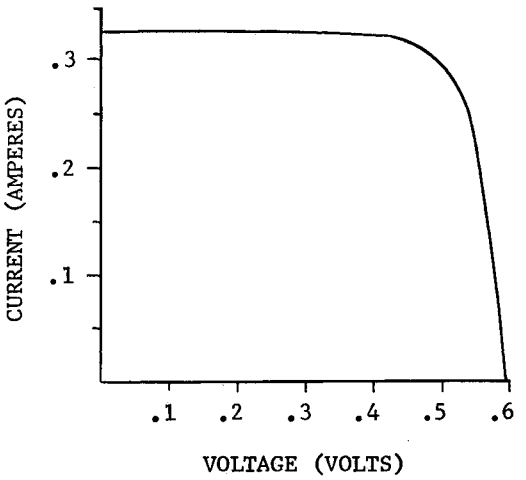

Fig. 4 Cell forward characteristic.

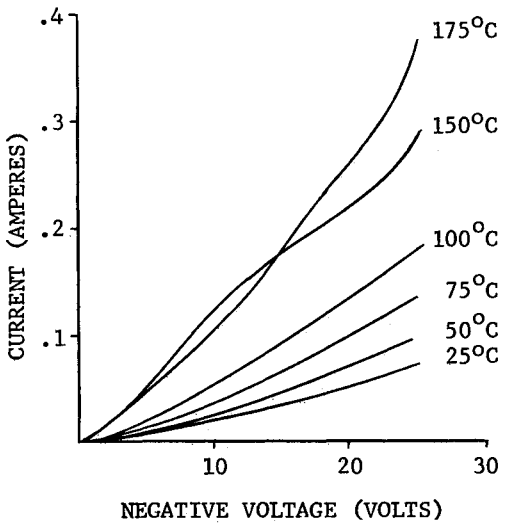

Fig. 5 Cell reverse characteristic.

To measure any array degradation as a result of the solar array "hot-spot" test, pretest array parameters were measured at a pulsed xenon solar illumination facility and recorded for a comparison with post-test parameters.

Solar Array "Hot Spot" Environmental Test Facility

The environmental chamber selected for the test was an optical physics laboratory's satellite component test facility. It was specifically designed for thermal and laser interaction studies. The chamber has been outfitted to provide the

following features: a vacuum on the order of 10^{-7} Torr, 100 K black walls, thermocouple and electrical feedthrough connectors, internally mounted infrared heaters for solar array pre- and post-test temperature control, ports equipped with salt windows for infrared monitoring devices, ports with quartz windows for solar simulator beam entry, and a rotating platform for solar array positioning with an indexed position indicator. The chamber is comprised of two smaller sections; the forward section is 1.2 m in diameter and 2.3 m in length, the rear section is 2 m in diameter and 2 m long. The chamber easily accommodates solar arrays of approximately 1 m square. Figure 6 is a sketch of the chamber.

A solar simulator was used to provide solar irradiation at the level of 1 AMO. The simulator radiation intensity and uniformity was measured using a silicon cell standard at the planned location of the solar array test specimen.

Infrared Scanner

The scanner employed was an AGA Thermovision 780, which converts electromagnetic thermal radiation from a viewed object into electronic video signals. The system consists of the following components: a scanner head comparable to a camera; a black-and-white monitor chassis with thermal range and level controls; a color monitor linked to the system via driver and receiver units; an OSCAR, which is an analog-to-digital converter with memory; and a magnetic tape recorder used to store and recall data and further process the records by a computer. The infrared image is converted into 256 levels subdivided from the selected thermal range.

Spatial resolution is determined by the scanner's field of view and the matrix of pixels in a record. There are 128 pixels along each scanner line and 128 scanner lines in each frame, thus there are 128×128 pixels in each record, each with 256 levels of thermal data. The time required for the scanner to complete a single picture frame is 0.16 s. The time used to digitize and record the frame on magnetic tape is 1.5 s.

Calibration Procedure

Although the infrared scanner is accompanied with a set of calibration curves by the manufacturer, the nature of the test and viewing constraints placed on the scanner make it necessary to recalibrate for this specific application.

Before the tests were initiated, the AGA Thermovision 780 system was calibrated to compensate for the KCl window and a 7 deg lens. A V-grooved, flat-surfaced black-body radiator and a conic cavity black-body radiator were used as the calibration sources. They were positioned at the same location in the environmental chamber that the array would occupy. The spectral transmission characteristics of the air/water vapor show high transmission in the region of detector/lens system sensitivity. Therefore, the air within the chamber was considered to have a negligible effect (see Fig. 7). Black-body temperatures were set at levels within the 45-155°C range. Throughout the calibration, a 1.8*f* aperture was used both with and without a 9 μm bandpass filter.

For each black-body temperature, the AGA 780 system was adjusted to center the black-body temperatures in the system range, which was 2 isotherm units (the most sensitive range). Digitized data from the AGA was taken and stored on magnetic tape. The thermal level and video voltages (related to the AGA's thermal level and overall radiation received at a particular range) were recorded by hand. A calibration graph was constructed to correlate the AGA thermovision level with the black-body temperatures (see Fig. 8). It was noted during the calibrating procedure that the apparent temperature, the AGA's thermal level and voltage, never dropped below 45°C, even though the actual black-body temperature was less. An effective temperature of 45°C was considered the baseline radiation level for this particular test configuration.

Correction for Emissivity

Before generating a correction curve to compensate for the solar cells' emissivity, it was important to evaluate the nature of the baseline temperature or thermal level. The baseline temperature was not related to the low-temperature measuring limits of the infrared scanner. Objects could be viewed directly (i.e., not through a window) and register an apparent temperature well under 45°C. The baseline temperature was due to background radiation related to viewing objects through a heated potassium chloride window.

Radiation emitted from either a black-body source or solar array in the chamber passes through the salt (KCl) window

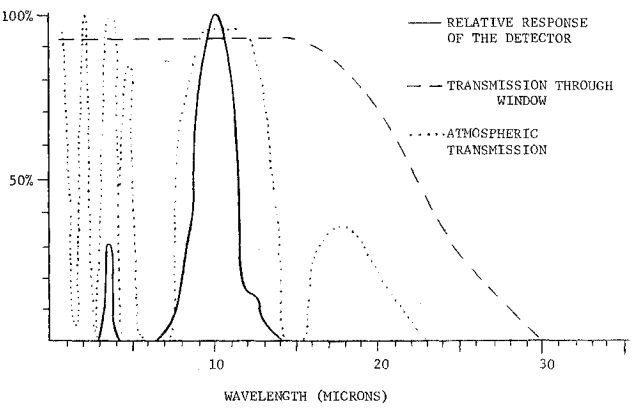

Fig. 7 Spectral transmission/response.

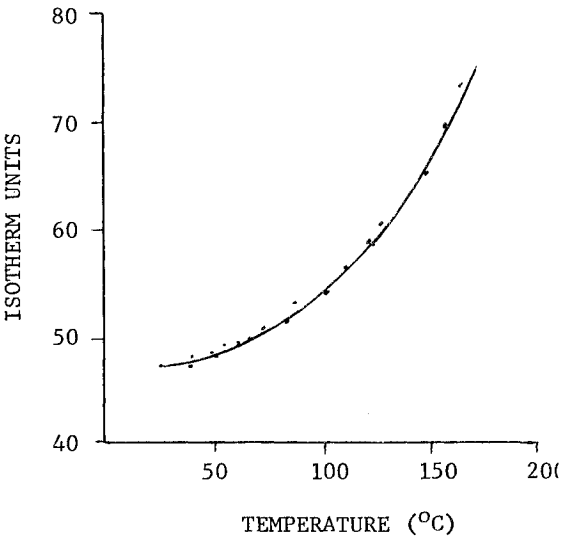

Fig. 8 Calibration curve.

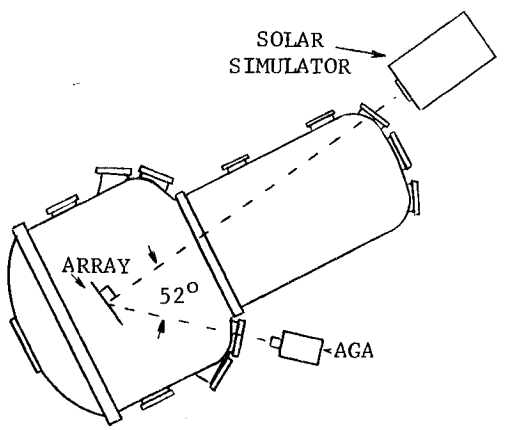

Fig. 6 Environmental chamber (top view).

before reaching the infrared scanner. At the surfaces of the window, a portion (8%) of the source radiation is back reflected and a small portion is absorbed by the air and salt. Radiation from the room also reaches the scanner by being reflected from the same salt window.

The heated salt window and air contribute to the background radiation, as does the room radiation reflected from the salt window. This postulation was supported when an increase in window temperature raised the baseline temperature. Figure 9 illustrates radiation paths from the sources to the infrared scanner. For purposes of calculating emissivity corrections to the calibration curve, the total radiation received by the infrared scanner is divided into two parts: 1) radiation from the black-body radiator or solar array and 2) radiation from all other sources (background radiation).

The radiation intensity seen by the infrared scanner when viewing a black-body radiator is calibrated to equal the radiation intensity emitted,

$$W_{dB} = W_B = \sigma T_B^4 \tag{1}$$

The balanced thermal level of an object viewed by the AGA 780 is the level where the object's thermal color is positioned about the zero isotherm. There is a 1:1 correspondence with the balanced thermal level and the radiation intensity the scanner receives. When the infrared scanner receives black-body radiation transmitted through a salt window, Eq. (1) is modified

$$W_{dB} = \tau W_B + W_{BG} \tag{2}$$

$$= \tau\sigma T_B^4 + \sigma T_{BG}^4 \tag{3}$$

Similarly, the radiation received by the infrared scanner when viewing a solar array is

$$W_{dA} = \tau W_A + W_{BG} \tag{4}$$

$$= \tau(\epsilon_A \sigma T_B^4) + \sigma T_{BG}^4 \tag{5}$$

When the temperature of the solar array is equal to the temperature of the black-body radiator, then

$$T_A = T_B \tag{6}$$

Solve Eq. (5) for T_A

$$T_A = [(W_{dA} - \sigma T_{BG}^4)/\tau\sigma\epsilon_A]^{1/4} \tag{7}$$

and solve Eq. (3) for T_B

$$T_B = [(W_{dB} - \sigma T_{BG}^4)/\sigma\tau]^{1/4} \tag{8}$$

Substitute Eqs. (7) and (8) into Eq. (6),

$$\left(\frac{W_{dA} - \sigma T_{BG}^4}{\tau\sigma\epsilon_A}\right)^{1/4} = \left(\frac{W_{dB} - \sigma T_{BG}^4}{\sigma\tau}\right)^{1/4} \tag{9}$$

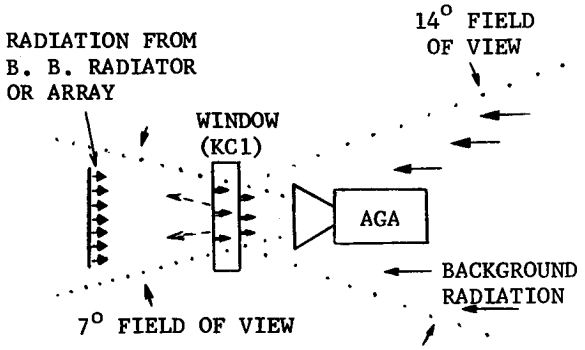

Fig. 9 Radiation paths from sources to infrared scanner.

Equation (9) then reduces to

$$W_{dA} - \sigma T_{BG}^4 = \epsilon_A W_{dB} - \epsilon_A \sigma T_{BG}^4 \tag{10}$$

Solve Eq. (10) for W_{dA}

$$W_{dA} = \epsilon_A (W_{dB} - W_{BG}) + W_{BG} \tag{11}$$

or

$$\sigma T_{dA}^4 = \epsilon_A (\sigma T_{dB}^4 - \sigma T_{BG}^4) + \sigma T_{BG}^4 \tag{12}$$

and solve for T_{dA}

$$T_{dA} = [\epsilon_A (T_{dB}^4 - T_{BG}^4) + T_{BG}^4]^{1/4} \tag{13}$$

The black-body calibration graph is used as an algorithm in conjunction with Eq. (13) to generate an emissivity corrected calibration graph (Fig. 10).

The step-by-step procedure used to generate the graph is:

1) Create a list of surface temperatures the solar array specimen is expected to achieve (50-250°C in increments of 5°C).

2) Use Eq. (13) to solve for T_{dA} for each value of T_{dB} in the list from step 1. $T_{BG} = 45$°C was obtained empirically and $\epsilon_A = 0.8$ is the solar cell emissivity determined by the manufacturer. The temperatures in the equation must be in deg Kelvin.

3) Using the calibration graph in Fig. 8, find the thermal levels associated with the temperature T_{dA}.

4) Plot the thermal levels vs the temperature T_{dB}, thus generating the emissivity corrected curve (middle curve in Fig. 11).

The errors involved in the correction graph revolve around the assumptions made regarding the stability of the background radiation and the emissivity of the solar array. If a 5°C error in measuring the background temperature is made, an error of 0.2°C results. If the background is not considered in the generation of an emissivity curve (bottom curve in Fig. 9), there may be a 20°C error introduced in the temperature measurement. The emissivity may not be constant in the infrared scanner's sensitivity range, but may vary with wavelength. Since the temperature of the array varies less than 200°C, treating the solar array as a grey body is a good approximation. The average emissivity of the array may not be precisely 0.8. If the emissivity were 0.82 instead of 80, there would be a corresponding error of 2°C in the 200°C region of solar array temperature and approximately 0.1°C in the low-temperature range.

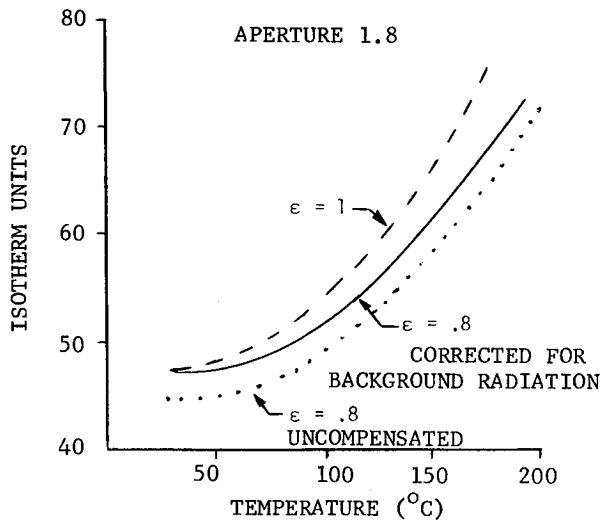

Fig. 10 Emissivity corrected calibration graph.

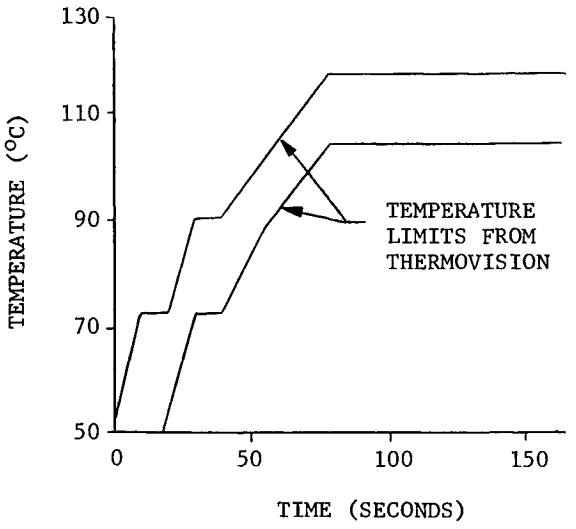

Fig. 11 Observed temperature of solar cell.

Hot-Spot Test Procedures

The array was mounted in the environmental chamber. All electrical and thermocouple connections to the array were made via the vacuum chamber feed-through port. The array was mounted so that its normal and center coincided with the center of the solar illumination pattern (nominally the chamber centerline). All electrical and thermal connections were verified before the chamber was evacuated and cryogenically cooled. The thermovision system was positioned at a diagnostic window with an aspect angle of 52 deg from the normal to the surface of the solar array. Solar reflections into the infrared scanner were consequently avoided.

The test specimen's *I-V* characteristic was plotted before and after most test conditions and at the completion of the tests. The "hot-spot" conditions were effected by opening, through remote switching, some of the solar cells. The surface temperature across the array was monitored by the Thermovision system and its digital representation was stored on magnetic tape. The laboratory computer monitored the warmup and cool-down phase of the testing via thermocouple signals.

The chamber was illuminated and the short circuit current of the last row of cells (the row with the faulting capability) was determined. A solar cell was then switched out of the circuit, simulating an open, while the current through the row was maintained at the short circuit level. Reverse biasing occurred in each of the remaining cells of that row. A record of the heating of the array was made every 10 s until it stabilized. Figure 11 presents two curves depicting the upper and lower temperatures present in a particular solar cell, as indicated by the color or colors of the cell at the time of observation.

Analysis

Construction of the Analytical Model

Since the faulted section of the array will have a common voltage, cells of different reverse characteristics will pass different currents. The reverse characteristics for the cells remaining in parallel with the open cell were constructed to conduct a worst-case analysis.

The design for a certain solar panel requires solar cell strings of 9, 10, 11, or 15 solar cells in parallel in the various solar cell circuits. The worst case would arise when one cell in nine opens. The eight remaining cells were modeled as: one cell having a very leaky reverse characteristic, thereby having a larger power dissipation, and seven average cells.

A graph was constructed for each individual solar cell in the array, which related its power dissipation as a function of temperature at the particular current it must pass in the singly faulted row. These dissipation curves as well as the initial temperatures, solar input, and thermal properties of a solar panel provide the input for a 135 node transient thermal model. The transient energy balance differential equation employed in the thermal program is as follows:

$$\underbrace{\frac{dT_i}{dt}}_{\text{rate of temperature change}} = \Big[\underbrace{s(\alpha_i - \eta_i)AI12_i\cos\theta_i}_{\text{solar flux}} + \underbrace{Q_i}_{\text{internal dissipation}} - \underbrace{\sigma\Sigma R_{ij}(T_i^4 - T_j^4)}_{\text{radiation coupling}} - \underbrace{\Sigma K_{ij}(T_i - T_j)}_{\text{conductive coupling}} - \underbrace{\sigma R I s_i T_i^4}_{\text{coupling to space}}\Big]\underbrace{\frac{1}{w_i C_{pi}}}_{\text{thermal capacitance}}$$

A cross section of that model is presented in Fig. 12.

Comparison

When the analysis results are plotted for the cell of interest in the faulted row along with the actual simulation results, Fig. 13 is obtained. This cell is the one with the fastest rising reverse characteristics, so its temperature would necessarily rise to the highest level. Comparing it to other cells in both the analysis and the test shows this to be true. Examination of Fig. 13 shows good correlation between the analytical model and the Thermovision observation. The thermal model prediction,

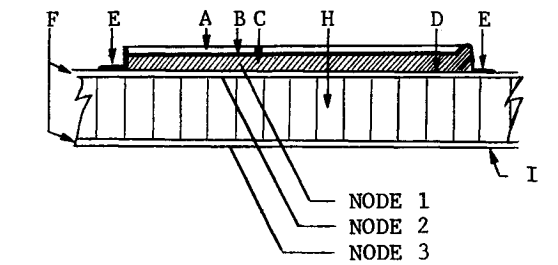

Fig. 12 Thermal model.

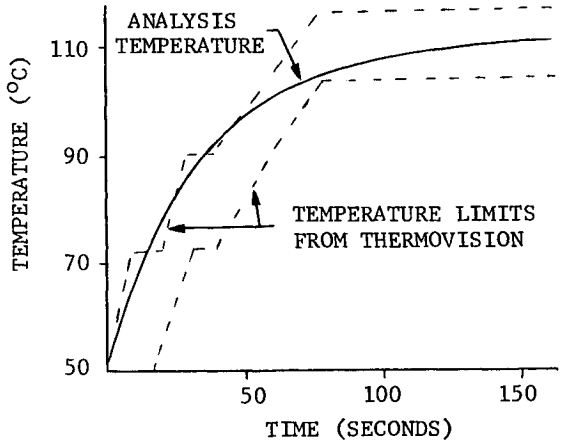

Fig. 13 Observed temperature and temperature from analysis.

after steady-state conditions have been reached, is within the tolerance band of the measuring system. Before a steady state has been achieved, a region of lesser importance, the predictions were slightly higher than the measured values.

Acknowledgments

The authors wish to thank Herbert Bilsky, Thomas Wylie, and Laura Goliaszewski of RCA Astro-Electronics and David Enlow, Lynn Minnich, and Taisa Dubinsky of G.E. Space Systems Division/RSO and Debra Rossi for their efforts and helpful discussions.

References

[1]Blake, F. A. and Hason, K. L., "The Hot Spot Failure Mode for Solar Arrays," *Proceedings of 4th IECEC,* AIChE, New York, Sept. 1969.

[2]Schneider, K. and Schultze, W. "The OTS Solar Array and the Solution of the 'Hot Spot' Problem," Paper presented at International Conference on Photovoltaic Power Generation, Hamburg, FRG, 1974.

[3]Gupta, A. and Milnes, A. G., "Effects of Shading and Defects in Solar Cell Arrays: A Simple Approach," Paper presented at 15th IEEE Photovoltaic Specialists Conference, 1981.

[4]Rauschenback, H. S. and Maiden, E. E., "Breakdown Phenomena in Reverse Biased Solar Cells," Paper presented at 9th IEEE Photovoltaic Specialists Conference, 1972.